Research Square

Preprints are preliminary reports that have not undergone peer review.
They should not be considered conclusive, used to inform clinical practice,
or referenced by the media as validated information.

Carrier excitation dynamics in black silicon nano pillar arrays

SEREF KALEM (seref.kalem@eng.bau.edu.tr)
Bahcesehir University https://orcid.org/0000-0002-0376-3615

Article

Keywords: Black silicon, quantum pillars, time-resolved photoluminescence, radiative recombination dynamics, interface traps, silicon sub-oxide, fast and slow states

Posted Date: September 24th, 2020

DOI: https://doi.org/10.21203/rs.3.rs-81652/v1

License: This work is licensed under a Creative Commons Attribution 4.0 International License.
Read Full License

Carrier excitation dynamics in black silicon nano pillar arrays

Seref Kalem

Bahcesehir University, Department of Electrical and Electronics Engineering, Faculty of Engineering and Natural Sciences, Besiktas, Istanbul, Turkey. e-mail: seref.kalem@eng.bau.edu.tr

Black silicon has attracted a great deal of interest for its promising photonic applications and exciting physical properties. Several approaches have been used to demonstrate the possibility of producing black silicon with CW light emission, but the investigation of a detailed radiative dynamical properties of the recombination process is still lacking. Here, we present ultrafast radiative recombination phenomena from black silicon consisting of quantum pillars produced by plasma ion etching. An ultrafast blue luminescence component competing with non-radiative recombination at surface defects was identified as no-phonon recombination process. This component involves two decay processes with a peak energy at around 480 nm, which have the fast component of about 10 ps followed by a component of around 50 ps decay time constant. The emission exhibits slow component in red spectral region with time constant ranging from 1.5 to 2.5 ns. When the surface of nano pillars is smoothed, the slow component at around 600 nm is enhanced to the detriment of blue-green emission, increasing the lifetime of carriers within the Si core of the quantum pillars. This process results in a slower sates assuming a 3-component exponential decay as measured by Streak camera. The ultrafast PL decay leads to a transfer of carriers to long-lived defect states as evidenced by a red emission at around 2 eV. The results are interpreted through the presence of quantum confinement at the tip regions of the pillars and surface defects originating from the oxide environment surrounding the nanometer size pillars.

Keywords— ***Black silicon; quantum pillars, time-resolved photoluminescence; radiative recombination dynamics; interface traps; silicon sub-oxide; fast and slow states.***

Black silicon (hereafter b-Si), a special form of silicon having a surface structure consisting of quantum size pillars formed as a result of surface etching using methods such as ultrafast laser pulsing of surfaces or reactive ion etching[1-7]. This form of Si has been the subject of significant attention due to its rich optical and electrical properties offering a great potential for promising applications for advanced scientific research subjects[8-10]. For solar energy harvesting applications through photovoltaic effect, black silicon surface is a perfectly compatible material with silicon solar cells providing a natural advantage with its ease of fabrication[11]. Solar cells fabricated using b-Si exhibited conversion efficiencies ranging from 10% up to 19% depending on the fabrication method[12-19]. Not only capturing the solar spectrum but also turning these pillars into field effect devices can offer a great advantage for sensor applications[20]. Light trapping can enable the realization of the photothermic conversion devices[21]. Isolating particles of interest within the forest of quantum nanosized pillars or using surface functionalizing techniques enables us to enhance the sensitivity while providing an advantage of filtering the particles to be detected[8,20]. Black silicon may find applications in imaging and micro-electro-mechanical systems (MEMS) as active and passive micro and nanostructured semiconductor quantum structures[22,23].

The surface formed on silicon wafers by above mentioned techniques consists of tapered pillars presenting quantum size structures down to a nanometer size tips[4]. It is interesting to see that the surface so obtained soaks all the visible light making the surface appear as a deep black color. Nevertheless, all those pillars were found to be crystalline as we have already demonstrated through transmission electron microscope (TEM) analysis[4]. However, the surfaces of these pillars are not atomically flat, representing some surface defects

like structure, missing atoms and oxidation induced capping regardless of wafer orientation. The presence of oxide cap layer or the oxidation of the surface of the pillars was also demonstrated by Fourier Transformed Infrared (FTIR) measurements of vibrational spectra. The presence of stretching modes of Si-O-Si vibrations at around 1090 cm^{-1} provides a clear evidence of the oxide formation at the surfaces of the pillars.

Owing to its quantum size surface structure, we have already reported an efficient continuous wave (CW) photoluminescence (PL) activity in a broad spectral range going from visible to near infrared region[4]. CW PL exhibits wafer (p-type or n-type), crystal structure and temperature dependent features both in the visible and in the near infrared region. In litterature, one can find a number of studies on time-resolved photoluminescence of silicon microstructures and nanostructures[24,25]. Despite several studies on CW photoluminescence and time-resolved PL on micro and nanostructures, there is no study on the radiative recombination dynamics of the quantum pillars in black Si. This work aims at filling this gap of exciting scientific and technological interest in such a surface.

Transformation of silicon surface to black silicon nanometer size pillars. The b-Si quantum pillars or whiskers were fabricated by a reactive ion etching (RIE) of thermally oxidized and photoresist (named as PMMA) coated 3 inch size p-type Si wafers having <100> and <111> crystal orientations as reported earlier[4]. Wafer resistivities used in the fabrication of b-Si in our work were around 10 Ω-cm. For the RIE of these wafers, we used chlorine plasma, which has led to the formation of quantum sized pillars on the surface of the Si wafer. Following this process, the wafer surface becomes black as appearance, since quantum pillars absorb all the white light turning the surface of the wafer to a deep black color.

High Resolution Transmission Electrom Microscopy (HRTEM) images. TEM studies on these wafers have shown that wafer surface consists of Si quantum pillars or whiskers type of extensions, which are aligned vertically to the wafer plane. As evidenced from the atom interference fringes observed in TEM as shown in Fig. 1a, these pillars are crystalline and their dimensions can be down to few atoms thick tips. On

their surface, some missing atom positions resulting in a certain irregular surface profile is visible. As shown in Fig. 1b their length can be up to 200 nm long with some core-shell like structure having a crystalline Si core, which is encapsulated by a surface oxide[4]. Within the Si core, regular atomic planes with inter atomic distances of 0.34 nm can be measured and the surface irregularities due to missing atoms are also visible. FTIR measurements in Fig. 1d indicate there is a native oxide on these pillars as evidenced from a relatively strong Si-O-Si absorption band related silicon-oxygen-silicon stretching vibrations at 1085 cm^{-1}.

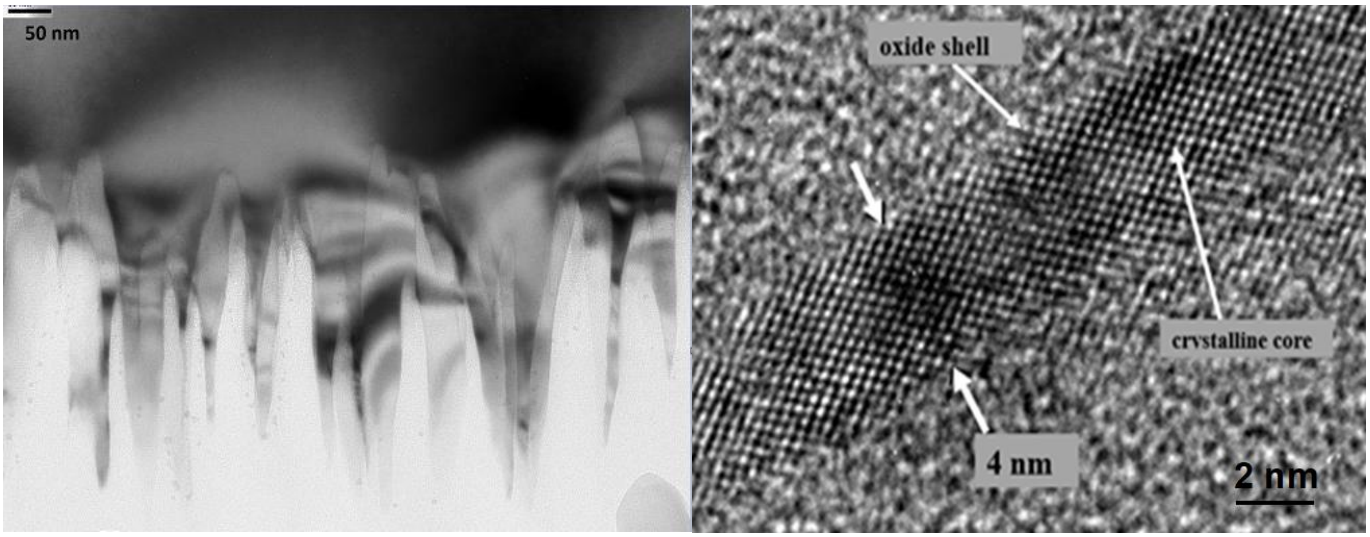
50 nm
oxide shell
crystalline core
4 nm
2 nm

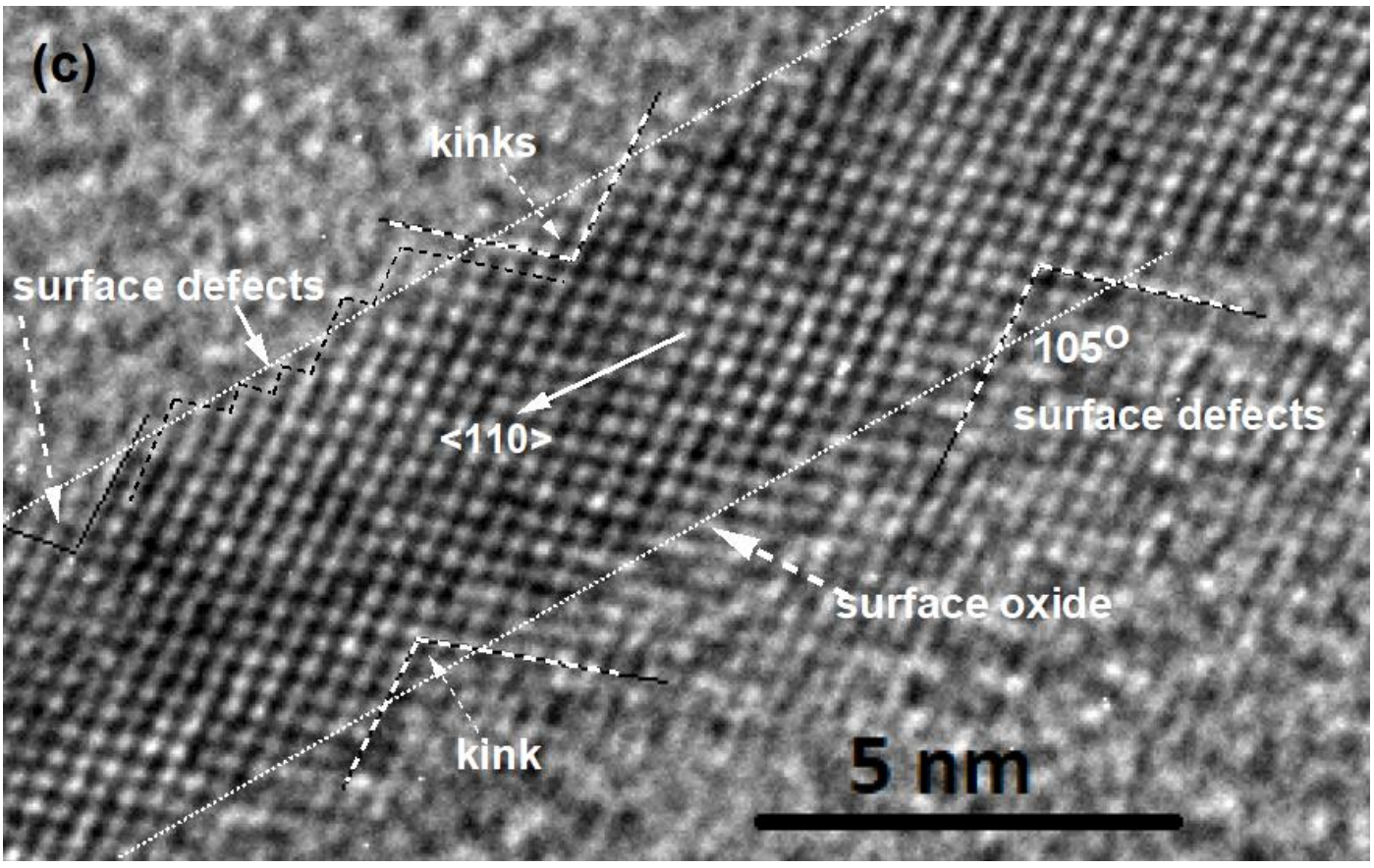
(c)
kinks
surface defects
<110>
105°
surface defects
surface oxide
kink
5 nm

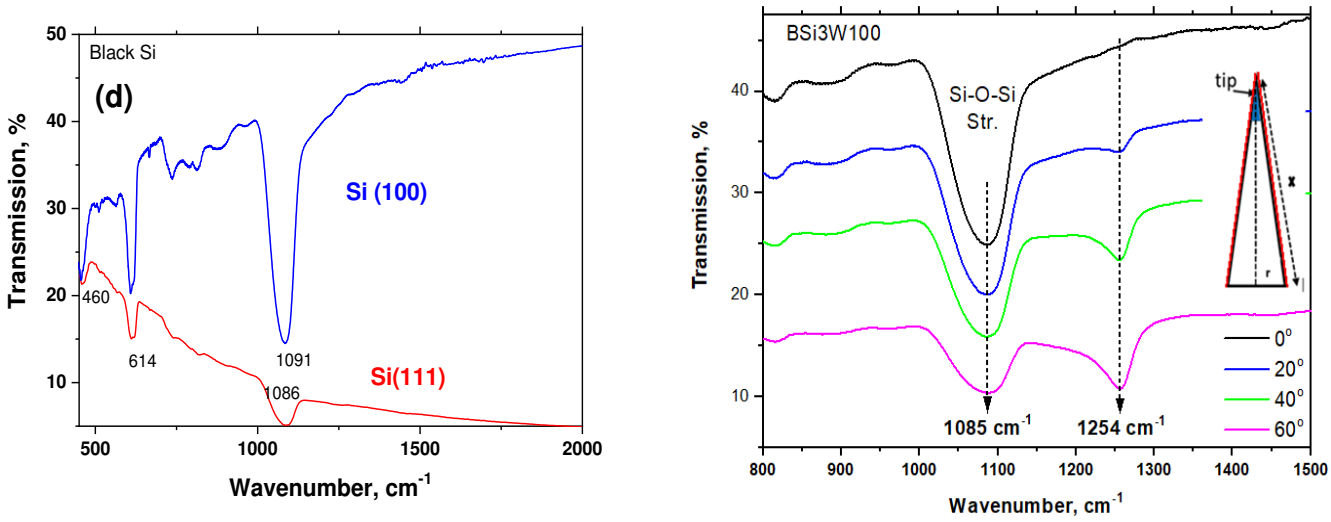

Fig.1| Transmission electron microscope image of black Si quantum pillars. **a**, TEM image of an individual quantum pillar, in which regular ordering of atoms and atom planes can be observed inside the crystalline structure. The surface of the quantum pillar is indicative of defects consisting of some interrupted planes and missing atoms. The oxide shell indicate an oxide layer of about ~1 nm on the pillar surface. **b,** TEM cross-sectional image at 50 nm magnification indicating an ensemble of quantum pillars vertically aligned to the wafer plane (100). **c**, Interface between the Si core and the oxide shell is separated with short length dots at both sides of the pillar. Ordering of individual atoms and crystallographic orientation along the pillar where the distances between atomic planes can readily be measured. The figure is typical of surface defects in the form of kinks as shown by angled lines. **d,** A typical FTIR spectrum of a black Si indicating the presence of oxidation as evidenced from the Si-O-Si stretching mode at 1085 cm^{-1}. **e**, The figure shows the incidence angle dependence of the Si-O-Si modes, revealing the appearance of some disorder coupled LO-TO phonon mode pairs at 1254 cm^{-1} as reported earlier [28]. The insert shows the geometry of an individual silicon pillar with the shaded tip region at the top where high energy photons are strongly absorbed. The oxide layer surrounding of the pillar is marked as red line capping the quantum structure.

FTIR spectra and localized vibrational modes. As shown in Fig.1d, b-Si exhibits a strong absorption band at 1085 cm-1, which originates from Si-O-Si symmetric stretching vibrations. This band is indicative of the presence of an oxide layer on the surface of the b-Si quantum pillars. From the close look at the surface details of a particular pillar, we observe that the surface oxidation does not form a measurable layer in TEM. The remaining significant peaks in the spectra are due to Transverse Optical (TO) phonon modes of Si at 460 nm, that is indicative of a disorder or amorphous like structure at the surface. The peak at 614 nm is the Si-Si phonon vibrations of the lattice. The insert shows the geometry of an individual silicon pillar with the shaded tip region at the top where high energy photons are absorbed. The oxide layer surrounding of the pillar is marked as red line capping the quantum pillar structure. Note that there is no vibrational features relating to hydrogen-silicon bondings as evidenced from the abscence of associated peak positions at around 2000-2000 cm-1. Fig.1d displays the incidence angle dependent transmission spectra of a b-Si. When the angle is increased, the strength of the band at 1085 cm^{-1} decreases in favor of the new band at 1254 cm^{-1}. We attribute this type of behavior to disorder induced splitting effects of LO-TO phonon modes as observed earlier[28].

Ultrafast radiative recombination dynamics and blue-green-red light emission. For the photoluminescence (PL) excitation dynamics, we used 100 femtoseconds Ti:Sapphire laser pulses at 400 nm as excitation wavelength and 80MHz repetition rates. The power of the excitation laser pulses was ranged from 100 μW to 8mW. The signal detection system used a Streak camera for ultrafast PL decays and a Time-Correlated Single Photon (TCSPC) measurement setups for the measurement of slow state decays.

Excited state dynamics of carriers ranging from blue to red spectral region were investigated by time-resolved photoluminescence (TRPL) at room temperature in b-Si consisting of high density quantum pillars whose dimensions are less than the de Broglie wavelength as evidenced from TEM images[4]. An ultrafast decay component of about 10-15 picosecond (ps) and a second fast component of around 30-50 ps

were deduced assuming a 3-components exponential decay process as measured by streak camera combined with TCSPC. The ultrafast PL decay results in a transfer of carriers to long-lived defect states as evidenced by a red emission at around 600 nm. Red shift at the initial stages of the blue luminescence decay confirms the presence of a likely charge transfer to long lived states. Time-correlated single photon counting measurements revealed a life-time of about 1.5-2.5 nanosecond (ns) for these states. We find that the same quantum structures emit also in the near infrared close to optical communication wavelengths. These results can be understood in terms of band structure modification at reduced sizes and defects induced at the surfaces involving dangling bonds and oxygen vacancies related radiative recombination centers in oxide on quantum pillars. The nature of the emission can be described considering confinement and traps, and modeling can thus be provided for the excitation dynamics of charge carriers.

Streak camera image. Figure 2 is a streak camera image of the emission from a b-Si consisting of a high density of quantum pillars. Black-Si was produced on p-Si(111) wafer. The streak camera image was taken using a laser excitation energy of 3.1 eV (400 nm). The apparent build up of the PL following the excitation is shown from 50 ps indicating a central intensity peak at around 490 nm. The temporal signal was attenuated very fast for times longer than 100 ps. Spectral intensity attenuates relatively fast at high energies and becomes weaker at longer wavelengths. For this sample blue-green PL is typical without the presence of any other spectral component. The spectral evolution of the PL exhibits a clear intensity distribution over the time scale explored. The spectrum beyond the 550 nm is at the almost full attenuation regime.

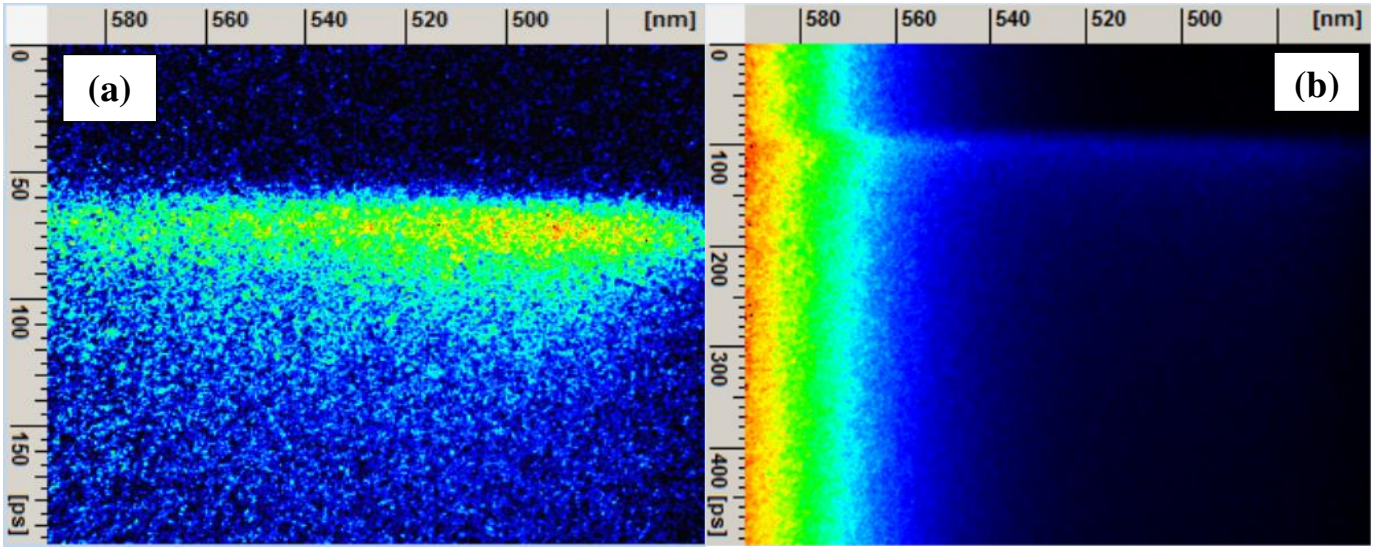

Fig. 2 | **Streak camera image of PL emission. a,** PL intensity distribution as taken from streak camera image of the blue-yellow emission of a b-Si, which was photoexcited at 400 nm (3.1 eV) and recorded for 200 ps following excitation process. Red-yellow colored regions indicate the strongest location of time-resolved emission. **b,** PL intensity distribution of b-Si quantum pillars, which were smoothed by exposing the surface to vapor of $HF:HNO_3$ acid mixture as explained elsewhere[30].

In order to determine the role of the oxide on the quantum pillars we have exposed the pillars to the vapor of $HF:HNO_3$ acid mixture[30]. The results are summarized in Fig. 2b, which shows the streak camera image for the treated b-Si sample. As shown in the image, the radiative recombination line peaks at around 100 ps and decays very fast right away from the ultra-fast emission line. The slower decay time in this surface smoothining process is probably indicative of the removal of defects on the surface of the pillars as evidenced from the slower decays in ultrafast radiative recombination regime.

Recombination dynamics. In Fig. 3, we observe the temporal and spectral evolution of the radiative recombination at 300K. The Fig.3a shows the amount of photon counting as a function of the decay time in picosecond at different wavelengths as deduced from the Fig.2. TRPL spectra were simulated by a curve

fitting program resulting in three components decay times as typical dynamical behavior of b-Si samples. For fitting the following expresssion was found to be well describing the luminescence decay

$$I\,(t) = \sum_i Ai\, e^{t/\tau_i}$$

where $A_i (i = 1, 2, 3)$ constants and τ_i is the decay time corresponding to the ultrafast component (around 10 ps), the decay time describing the non-radiative recombination at the Si core surface defects or Si core-silicon oxide cap layer (50 ps) and a slow component (1.5-2.5 ns) characterizing radiative decay time through oxygen related defects whithin the surface oxide surrounding quantum pillars, respectively.

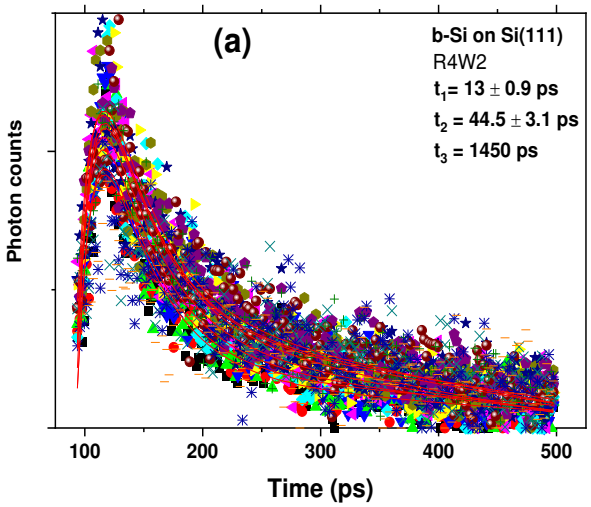

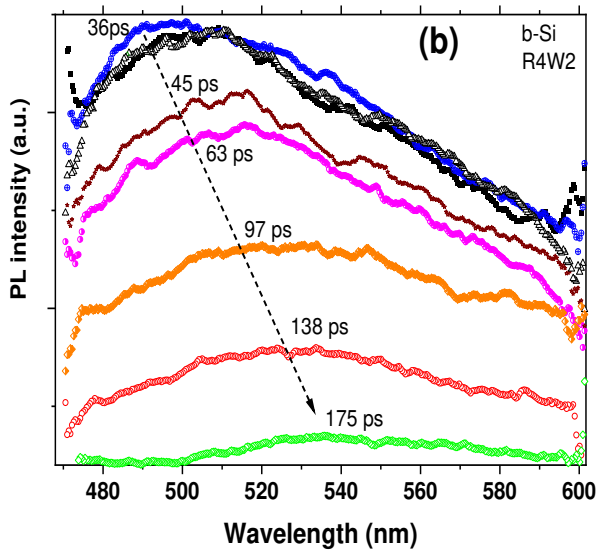

Fig. 3 | Room temperature excitation dynamics at 300 K. **a**, Time-resolved PL spectra integrated from 450 nm to 600 nm b-Si. The solid red lines indicates a global fitting of the dynamics to a triple exponential decay functions. **b**, Spectral distribution of PL between 470 nm and 600 nm taken at different radiative recombination decay times. As shown in Fig.3b, the peak position of the time dependent emission shifts toward the longer wavelengths, indicating the charge transfer to slower states.

In order to verify the effect of any quantum confinement, we assume a nanowire or quantum dot like confinement structures, which may be responsible for the ultrafast component of the light emission at around 480 nm. These dots can be expected to be located at the tips of the pillars as evidenced from the TEM results. Following the analysis made previously[34], a quantum dot structure can confine electrons in three directions whithin a volume of d_1, d_2, d_3. The confinement energy can then be expressed in the following form: $E = E_c + E_{q1} + E_{q2} + E_{q3} + \frac{\hbar^2 k^2}{2m_c}$, where $E_{qi}=\frac{\hbar^2 \pi^2}{2m_c}(\frac{q_i^2}{d_i^2})$ with q_i=1, 2, 3,... quantum number and d_i=d_1, d_2, d_3 are the unit length of the box in three dimensions and k is the vector component. Assuming $d_1=d_2=d_3$ and k=0, $E = E_c + 3E_q$ where $E_q=E_{q1}=E_{q2}=E_{q3}$ and E_c=1,1 eV as the bandgap of the bulk Si. $E_q = 2{,}89\text{x}10^{-18}$ eV.m^2 (1/d)^2 where d is in nm, E_q is the confinement energy. From these estimations, we find that the ultrafast component of the emisssion is probably originating from the Si volume size of about d = 2.5 nm, that is 15,6 nm^3. Size dependent change of the confinement energy is shown in Fig. 4b as an insert.

Smoothing of nano pillar surfaces. It has already been shown that the exposure of silicon rods to the vapor of an acid mixture containing HF and HNO_3 has the effect of smoothing the surface of the rods[30]. Similar effects are expected for the b-Si quantum pillars. Therefore, the PL decay measurements have beeen performed also on b-Si quantum pillar samples, which were subjected to the surface smoothing procedure as described earlier[30]. This procedure removes some of the oxide from the shell region on the pillar surfaces.

The results obtained from these investigations on such samples are displayed on Fig.4 for a b-Si quantum pillar formed on p-Si(100). The findings are indicative of an increase in carrier lifetimes in b-Si quantum pillars, which have been subjected to surface smoothing process. This process removes the surface oxide but at the same time initiates a new oxide growth on the surface. This process can be interpreted as a surface smoothing removing of defects such as kinks while eliminating traps at the interface between the shell and the oxide layer encapsulating silicon pillars. As shown on Fig. 4a, the stertched PL decay curves of etched pillars resulted in rather longer time-contants, that is 12,7 ps, 30,9 ps and a slower component of 4500 ps as compared to as-fabricated b-Si quantum pillars. This effect can be attributed to the fact that the surface smoothing passivates some of the traps at the surfaces and the enhancement of oxidation increases the life-time of the carriers.

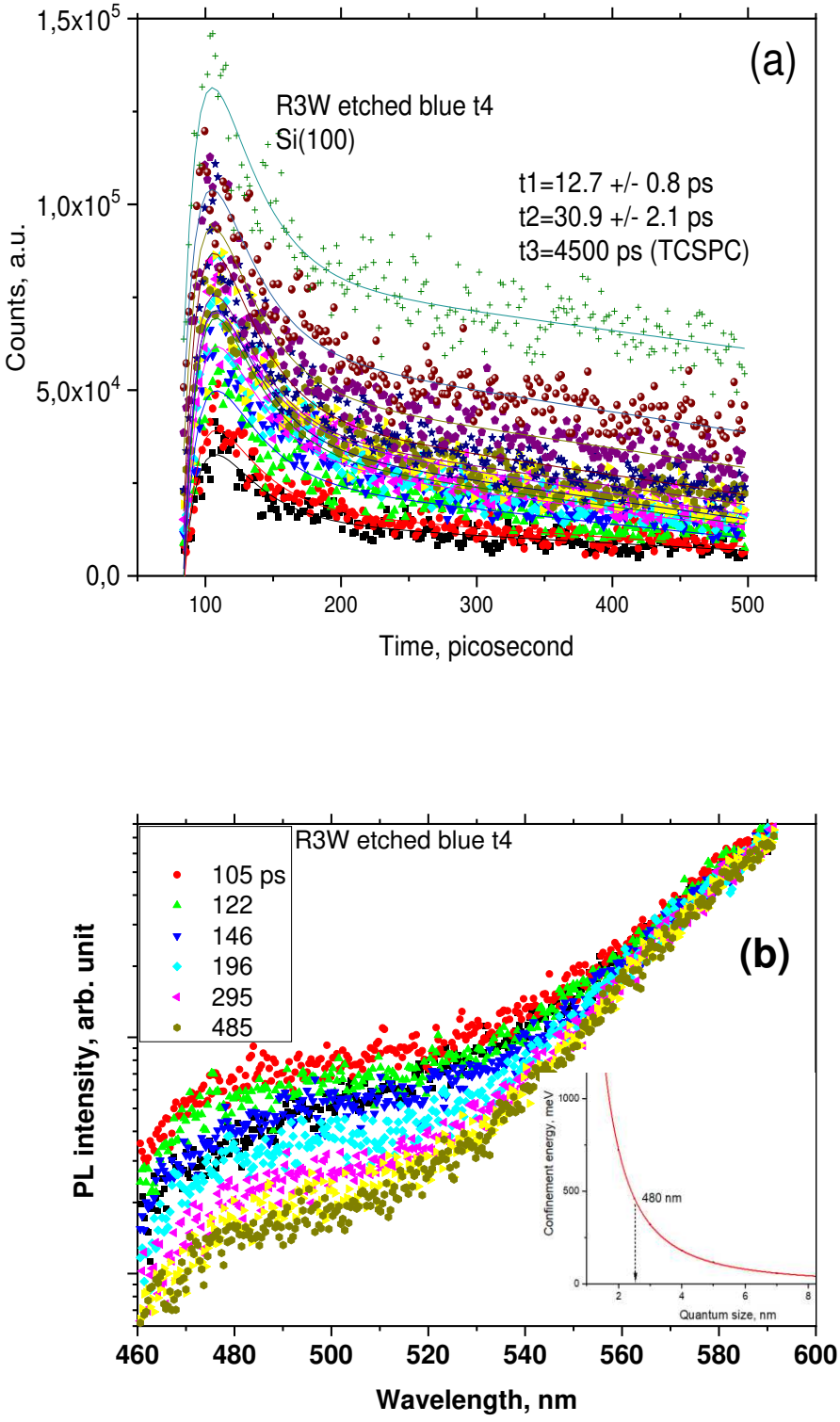

Fig. 4 | Room temperature excitation dynamics at 300 K for quantum pillars treated by HF:HNO$_3$ vapors. **a**, Time-resolved PL stretching spectra integrated from 450 nm to 600 nm of b-Si. The solid red

lines indicate a global fitting of the dynamics to a triple exponential decay functions. **b**, Spectral distribution of PL spectra between 470 nm and 600 nm as taken at different times.

Time-correlated single photon counting. Figure 2 shows the time-resolved PL dynamics spectrally integrated from 450 nm to 600 nm for a black-Si produced on Si(111) as a function of decay time. The solid lines indicates a global fitting of the PL dynamics to a triple exponential decay functions. As indicated in Fig.2, the blue emission at around 480 nm corresponds to the fast decay component of about 10 ps timeframe. This component could be attributed to direct transistions whithin the quantum pillars due to the size reduced enhancement of the overlapping of the electron and hole wave functions leading to strongest oscillator strength. The fitting leads also to the presence of a component in the order of few nanoseconds corresponding to slow states induced probably by surface defects such as Si vacancies in the oxide layer surrounding quantum pillars. An intermediate decay time of about 50 ps could be due to re-excitation of thermalized carriers or recombination in non-radiative traps at the interface between the silicon core and surface oxide layer. TCSP measurements revealed decay times ranging from around 1.5 ns up to 2.5 ns time range, which are attributable to vacancies in oxide layer.

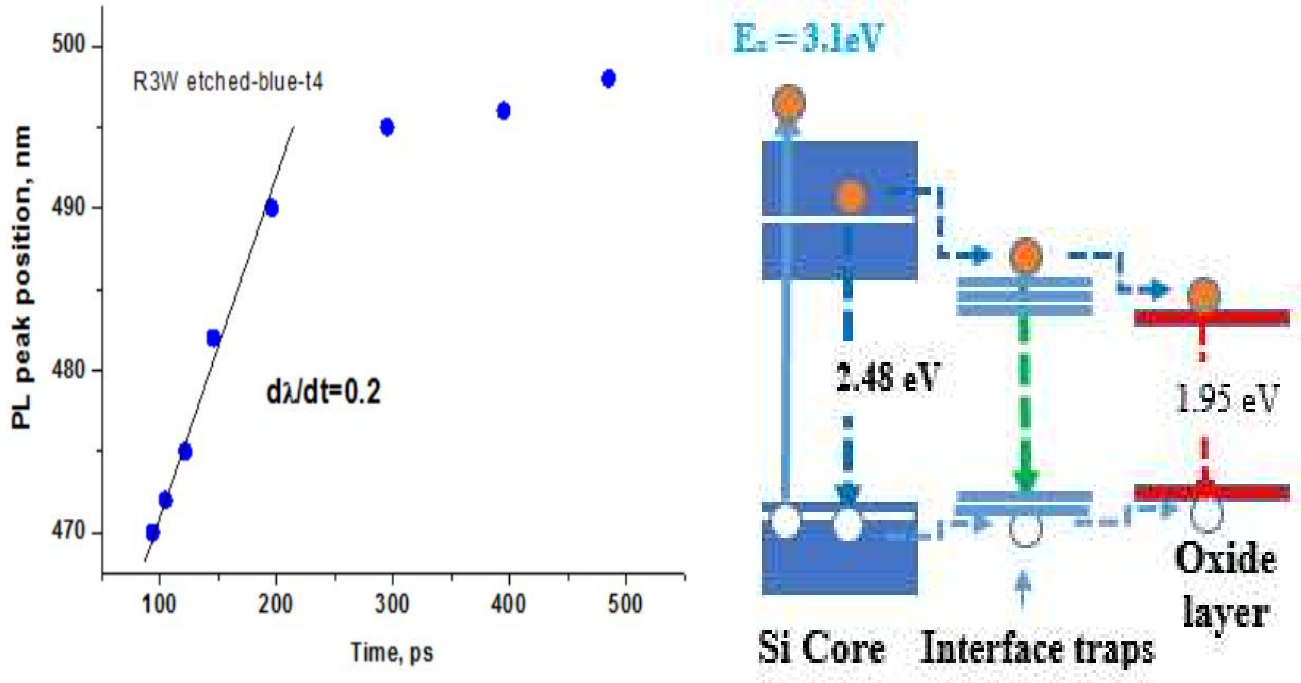

Fig. 5| First derivative of the peak position versus decay-time. a, PL peak position as a function of decay time exhibits two slopes for the change. The change rate $^{d\lambda}/_{dt} = 0.2$ over fast states is much higher than that for the slower states, that is $^{d\lambda}/_{dt} = 0.019$, which is the typical characteristic of the slower states. **b,** Energy band diagram indicating the involvement of three states taking part in the recombination kinetics. The left hand side is the silicon core where the blue-green emission at around 2.5 eV occur due to the confinement effect; the middle part indicates traps involved recombination due to localized states between the core and the surface oxide; the right hand side is the red recombination originating from the oxide around the pillars.

Non-radiative recombination at traps was shown to be playing a significant role in photoluminescence decay in semiconductors[4]. Threrefore, the intermediate decay component of around 50 ps could be attributed to the presence of traps at the surfaces of quantum pillars. Radiative or non-radiative recombination at these

traps are expected to play a significant role in determining the magnitudes of the decay time components in b-Si. While the non-radiative recombination reduces the emission intensity, the radiative one contributes to the spectral region between the blue and the red region.

From these results, we observe that the intensity of light emission at around 480 nm resulting from the ultrafast decay is rather weak. The reason of this can be the following: 1) quantum size concerns only the tip regions of relatively small volume as compared to the whole pillar volume, 2) electron-hole pair generated at the tips of the quantum pillars diffuses fast away from the tip regions to trap states or larger dimensional parts of the silicon core thus reducing the rate of the quantum confined radiative recombination of carriers. These processes are likely at the origin of the weak emission at around 480 nm. The most of the excitation light is absorbed in the remaining parts of the pillars thus contributing light emission originating from the slow states at around 600nm. A typical shape of a pillar can be assumed to be a cone with a height of about 250 nm and with a cone diameter of around 100 nm as shown at the insert in Fig. 1d. The surface area of such a pillar can be estimated from $A = \pi r x$, where r and x are the radius and the length of the lateral surface, respectively. Using these parameters, the surface area of the pillar can be estimated to be $A \approx 4\text{x}10^4\ nm^2$ as compared to a tip region of 5 nm in size having a surface area of around 100 nm, leading to a ratio of surface area of about 400. This comparison indicates that actually a very small part of the light excitation occurs within the quantum sized region of the tip of the pillar. This explains why the photoluminescence intensity is weak and the decay times are fast at high energies corresponding to tip regions where quantum size effects are expected. Beside the small volume of the tip regions, diffusion of generated electron-hole pairs from these regions toward the bulk part of the pillars play also a significant role in the strength of the high energy component of the time-resolved PL.

As shown in Fig. 5a, the PL peak position shift rate $d\lambda/dt$ is much slower in etched b-Si than as-fabricated one, which is indicative of a very fast charge transfer in b-Si. These findings suggest that the acid vapor treatment removes fast states, which are likely more effective at the tip regions of the pillars, where quantum

confinement effects are dominant. Secondary effect of the vapor treatment is to enhance the oxidation around the core silicon pillar. The enhancement of the PL intensity of the long lived states in etched samples supports this type of evolution in recombination dynamics. Due to variable peak positions ranging from 470 nm to 540 nm, we attribute this band to hot carrier non-phonon emission originating from the core silicon, that is the tip region of the pillars. Thus, the short-lived component of about 5-15 ps could well be associated with the lifetime of these carriers, which are fast recombined at the interface traps between the shell and the oxide surrounding.

Conclusions and outlook. We have presented a method to deduce the individual excited state decay components in a black silicon and analyzed the data in order to identify the origin of the radiative recombination process. We find that there is an ultrafast decay of excited carriers at around 480 nm with about 10 ps decay time constant, a blue-green emission close to femtosecond regime due to non-phonon electron-hole recombination within the quantum pillars. This decay component is followed by a slow component in red spectral region, indicating a very fast charge transfer of carriers in black silicon nano pillars. The slow component time decay can range from 1.5 ns to 2.5 ns as evidenced from the time correlated single photon measurements. Recombination component at intermediate time scales of around 50 ps can be attributed to trap states where non-radiative recombination is a dominant effect at the interface between the core and the surface oxide of the quantum pillars. We have shown when the surfaces of the b-Si nano pillars are smoothed by acid vapor treatment, the decay-time constants become larger, which is indicative of a decrease in surface defect states.

From these studies, we have shown that silicon nano pillars in black silicon exhibit exciting optical properties, which offer promising application possibilities in ultra large scale integration of sensors, memory, switching devices, imaging, energy harvesting, quantum hardware fabrication for quantum technologies and optical information processing platform integrating near infrared optoelectronic components.

ACKNOWLEDGMENTS

This work was supported by European Commission LASERLAB-EUROPE program (LLC001765). We thank Prof. W. Sunström for the access to Lund Laser Center and Dr.A.E. Hannas for the assistance in laser measurements. The BMBF–TUBITAK bilateral program under contract No: 107T624, and the German Federal Ministry of Education and Research (Grant No: 03Z2HN12). We thank Dr. P. Werner for HRTEM measurements and fruitful discussions.

References

1. Oerlein , G. S. & Kurogi,Y. Sidewall surface chemistry in directional etching processes. Materials Science and Engineering **24**, 153 (1998).
2. Gotza, M., Dutoit, M. and Ilegems, M. Formation of nanoscale columnar structures in silicon by a maskless reactive ion etching process. *J. Vac. Sci. Technol.* **B 16**, 582 (1998).
3. T. Chen, J. Si, X. Hou, S. Kanehira, K. Miura and K. Hirao. Luminescence of black silicon fabricated by high-repetition rate femtosecond laser pulses. J. of Applied Physics **110**, 173106 (2011).
4. Kalem, S., Werner, P., Arthursson, O., Talalaev, V., Nilsson, B., Hagberg, M., Frederiksen, H. & Sodervall, U. Black silicon with high density and high aspect ratio nano whiskers. Nanotechnology **22**, 1 (2011).
5. Liu, X et al, Black silicon: fabrication methods, properties and solar energy applications. Energy Environ. Sci. 7, 3223(2014).
6. Kontermann, S et al. Laser processed black silicon for photovoltaic applications. Energy Procedia **27**, 390 (2012).
7. Toor, F. et al. Nanostructured silicon via metal assisted catalyzed etch (MACE): chemistry fundamentals and pattern engineering. Nanotechnology **27**, 41 (2016).

8. Weiss, P. W., Bissig, B., Feurer, T., Carron, R., Buechler, S. & Tiwari, A. N. Bulk and surface recombination properties in thin film semiconductors with different surface treatments from time-resolved photoluminescence measurements. Scientific reports **9**, 1-13 (2019).

9. Lu, P., Li, D., Zhang, P., Tan, D., Mu, W., Xu, J., Li, W. & Chen, K. Time-resolved and temperature dependent photoluminescence study on phosphorus doped Si quantum dots/SiO2 multilayers with ultra-small dot sizes. Optical materials Express **6**, 3233 (2016).

10. Serpenguzel, A., Kurt, A., Inanc, I., Cary, J. E. & Mazur, E. Luminescence of black silicon. Journal of Nanophotonics **2**, 021770 (2008).

11. Koynov, S., Brandt, M. S. & Stuttzmann, M. Black nonreflecting silicon surfaces for solar cells. Applied Physics Letters **88**, 203107-1 (2006).

12. Rabha, M. B., Anouar, H. & Brahim, B. Solar Energy **86**, 1411–1415 (2012).

13. Toor, F., Branz, H. M., Page, M. R., Jones, K. M. & Yuan, H. C. Appl. Phys. Lett. **99** 103501 (2011).

14. Liu, Y., Lai, T., Li, H., Wang, Y., Mei, Z., Liang, H., Li, Z., Zhang, F., Wang, W., Kuznetsov, A. Y. & Du, X. Small **8**, 1392–1397 (2012).

15. Zhao, Z., B. Zhang, P. Li, W. Guo and A. Liu, Int. J. Photoenergy, 2014, 2014, 683654.

16. Liu, Y., A. Das, Z. Lin, I. B. Cooper, A. Rohatgi and C. P. Wong, Nano Energy, 2014, 3, 127–133

17. Yang, L., Y. Liu, Y. Wang, X. Li, W. Chen, Y. Hua, Q. Zhang, J. Fu, H. Liang, Z. Mei and X. Du, RSC Adv.**4**, 24458– 24462 (2014).

18. Jura, M.P. et al. Conventionally-processed silicon nanowire solar cells demonstrating efficiency improvement over standard cells. Photovoltaic Specialist Conference (PVSC), 2014 IEEE 40th, 2014.

19. Wang, X. et al. 19.31%-efficient multicrystalline silicon solar cells using MCCE black silicon technology, Photovoltaics International **35**, March 2017.

20. Mironenko, A. Y., M.V. Tutov, A.A. Sergeev, E.V. Mitsai, A.Y. Ustinov, A. Y. Zhizhchenko, D. P. Linklater, S.Y. Bratskaya, S. Juodkazis, A.A. Kuchmizhak. Ultratrace nitroaromatic vapor detection via surface-enhanced fluorescence on carbazole-terminated black silicon. *ACS Sens.* **4**, pp.2879-2884, 2019.

21. Zhang Z et al., Black silicon with order-disorder structures for enhanced light trapping and photothermic conversion, Nano Energy **65**, 103992 (2019).

22. Lv, J., T. Zhang, P. Zhang, Y. Zhao, S. Li, Review application of nanostructured black silicon. Nanoscale Research Letters **13:110**, 2 (2018).

23. Tan, Q., F. Lu, C. Xue, W. Zhang, L. Lin, J. Xiong, Nano-fabrication methods and novel applications of black silicon, Sensors and Actuators A:Physical **295**, 560-573 (2019).

24. Zidek, K, F. Trojánek, P. Malý, L. Ondič, I. Pelant, K. Dohnalová, L. Šiller, R. Little, and B. R. Horrocks, Femtosecond luminescence spectroscopy of core states in silicon nanocrystals, Opt. Express **18**, 25241(2010).

25. Chen, Z et al. Time-resolved photoluminescence of silicon microstructures fabricated by femtosecond laser in air. Optics Express **21**, 21329 (2013).

26. Schmidt, T., A. I. Chizhik, A. M. Chizhik, K. Potrick, A. J. Meixner, and F. Huisken. Radiative exciton recombination and defect luminescence observed in single silicon nanocrystals. Phys. Rev. B **86**, 125302 (2012).

27. Zidek, K et al., Ultrafast photoluminescence dynamics of blue-emitting silicon nanostructures, Phys. Status Solidi C **8**, 979 (2011).

28. Kalem, S. et al. Optical characterization of dislocation free Ge and GeOI wafers, Materials Science in Semiconductor Processing **9**, 753(2006).

29. Strubbe, D. A., E.C. Johlin, T.R. Kirkpatrick, T. Buonassisi, and J. C. Grosman. Stress effects on the Raman spectrum of an amorphous materials:Theory and experiment on a-Si:H. Physical Review **B 92**, 241202 (2015).

30. Kalem, S., P. Werner, B. Nilsson, V.G. Talalaev, M. Hagberg, Ö. Arthursson, U. Södervall. Controlled thinning and surface smoothening of Silicon nanopillars. Nanotechnology **20**, 445303-7 (2009).

31. Wu Z., Neaton, J.B. and Grossman, J.C.. Quantum confinement and electronic properties of tapered silicon nanowires, Physical Review Letters 100, 246804(2008)

32. Green, M.A. J. Appl. Phys. Intrinsic concentration, effective densities of states and effective mass in silicon. J. Appl. Phys.**67**, 2944(1990).

33. Ma, D.D.D., et al. Small diameter silicon nanowire surfaces. Science **299**, 1874(2003).

34. Saleh, B.E.A. and Teich, M.C. Fundamentals of Photonics. 3rd Ed.,Wiley series in pure and applied optics, 760 (2019).

Figures

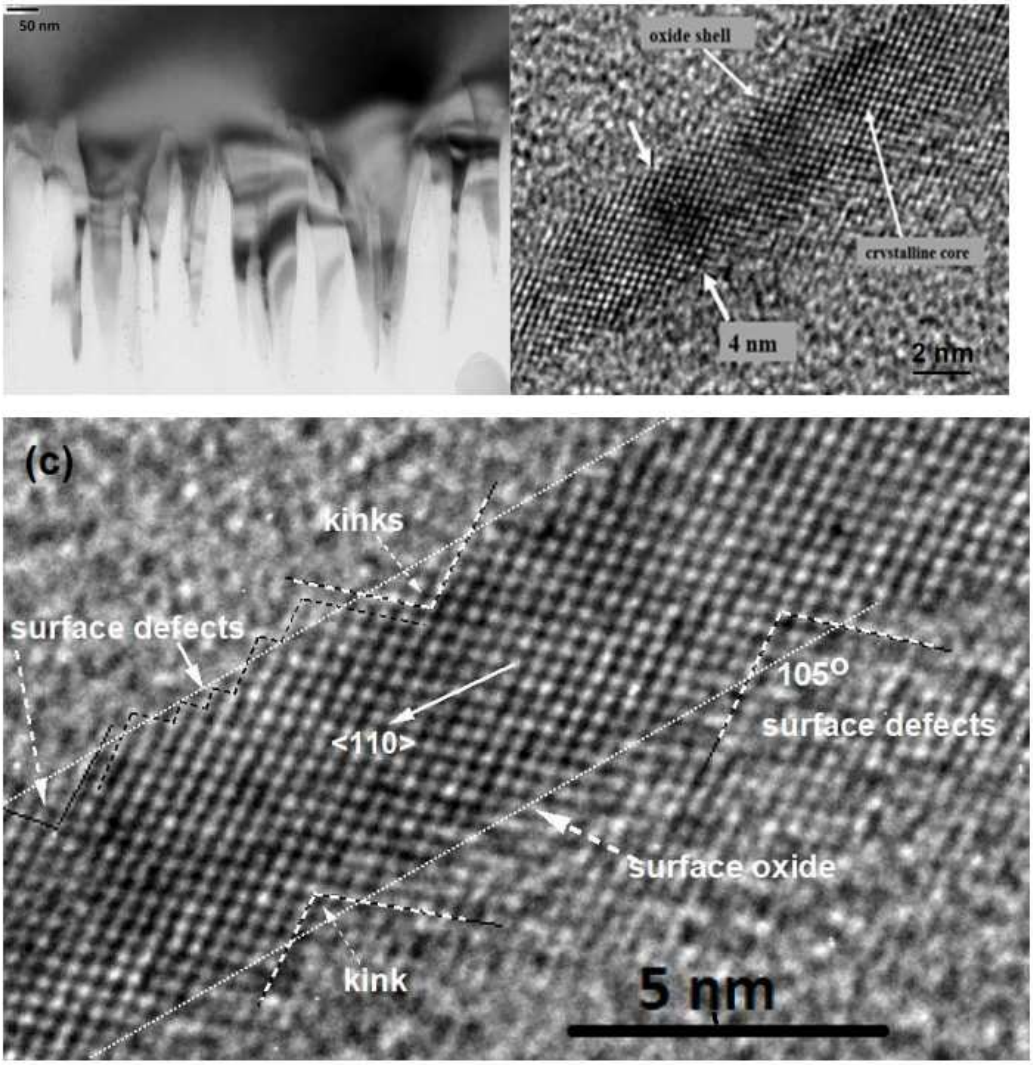

Figure 1

Transmission electron microscope image of black Si quantum pillars. a, TEM image of an individual quantum pillar, in which regular ordering of atoms and atom planes can be observed inside the crystalline structure. The surface of the quantum pillar is indicative of defects consisting of some interrupted planes

and missing atoms. The oxide shell indicate an oxide layer of about ~1 nm on the pillar surface. b, TEM cross-sectional image at 50 nm magnification indicating an ensemble of quantum pillars vertically aligned to the wafer plane (100). c, Interface between the Si core and the oxide shell is separated with short length dots at both sides of the pillar. Ordering of individual atoms and crystallographic orientation along the pillar where the distances between atomic planes can readily be measured. The figure is typical of surface defects in the form of kinks as shown by angled lines. d, A typical FTIR spectrum of a black Si indicating the presence of oxidation as evidenced from the Si-O-Si stretching mode at 1085 cm-1 . e, The figure shows the incidence angle dependence of the Si-O-Si modes, revealing the appearance of some disorder coupled LO-TO phonon mode pairs at 1254 cm-1 as reported earlier 28. The insert shows the geometry of an individual silicon pillar with the shaded tip region at the top where high energy photons are strongly absorbed. The oxide layer surrounding of the pillar is marked as red line capping the quantum structure.

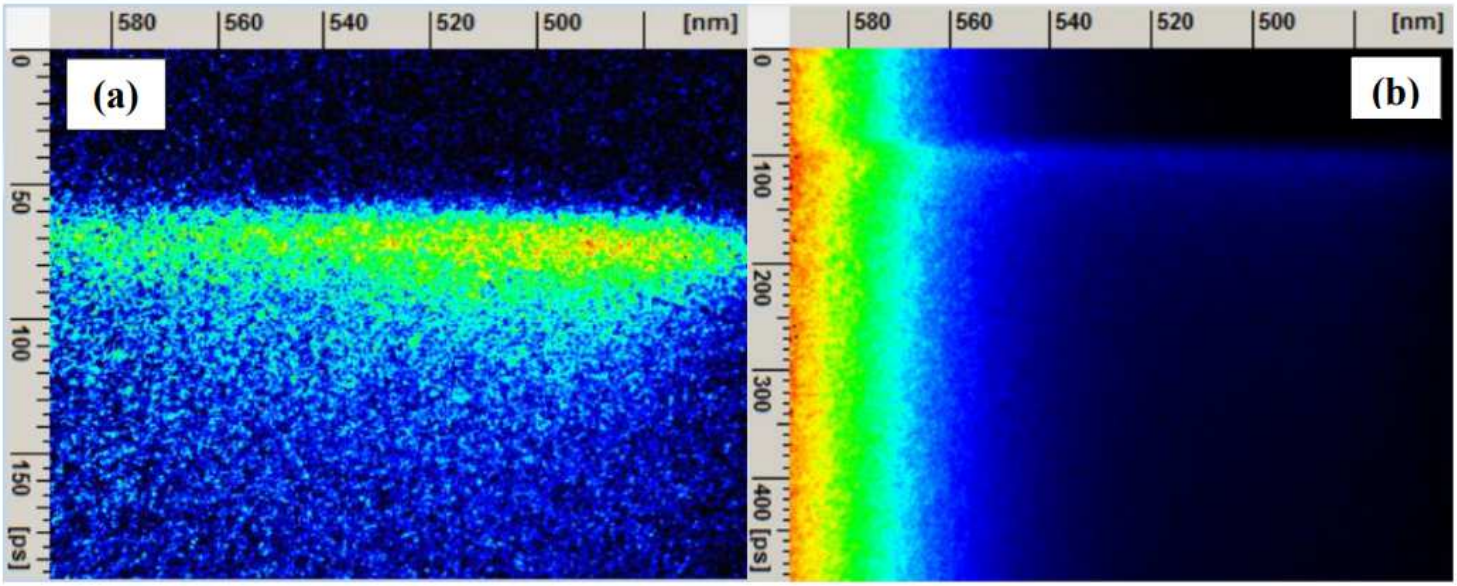

Figure 2

Streak camera image of PL emission. a, PL intensity distribution as taken from streak camera image of the blue-yellow emission of a b-Si, which was photoexcited at 400 nm (3.1 eV) and recorded for 200 ps following excitation process. Red-yellow colored regions indicate the strongest location of timeresolved emission. b, PL intensity distribution of b-Si quantum pillars, which were smoothed by exposing the surface to vapor of HF:HNO3 acid mixture as explained elsewhere30 .

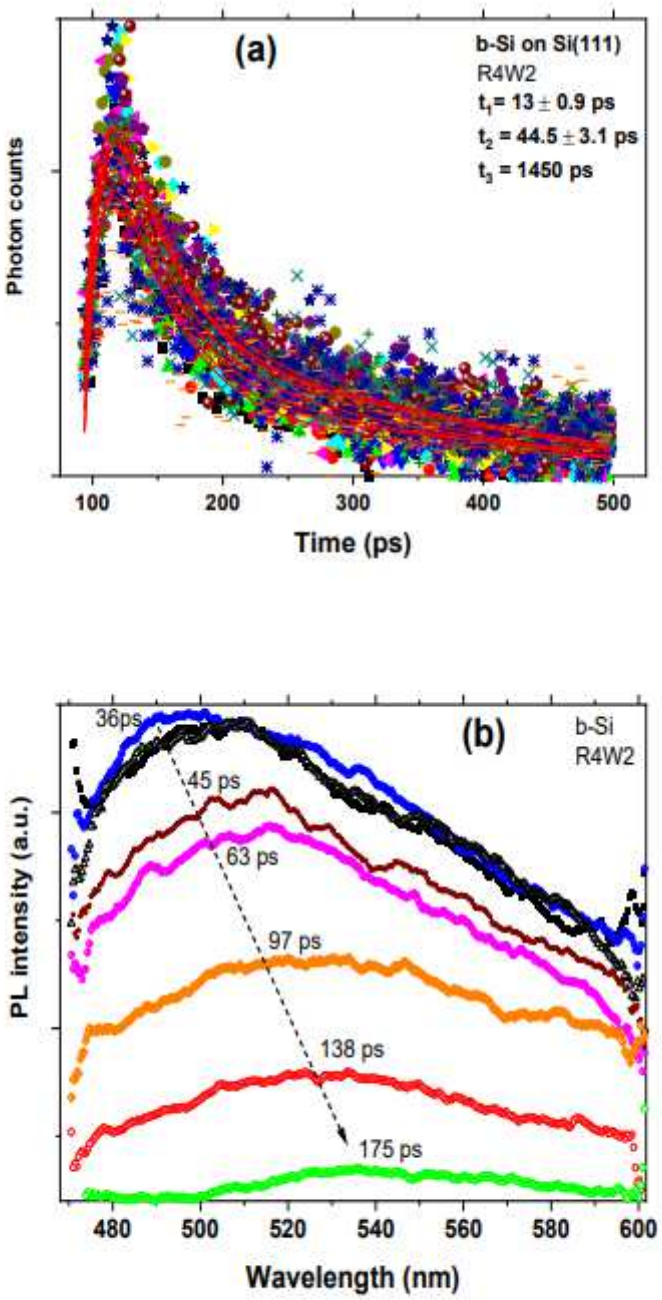

Figure 3

Room temperature excitation dynamics at 300 K. a, Time-resolved PL spectra integrated from 450 nm to 600 nm b-Si. The solid red lines indicates a global fitting of the dynamics to a triple exponential decay functions. b, Spectral distribution of PL between 470 nm and 600 nm taken at different radiative recombination decay times. As shown in Fig.3b, the peak position of the time dependent emission shifts toward the longer wavelengths, indicating the charge transfer to slower states.

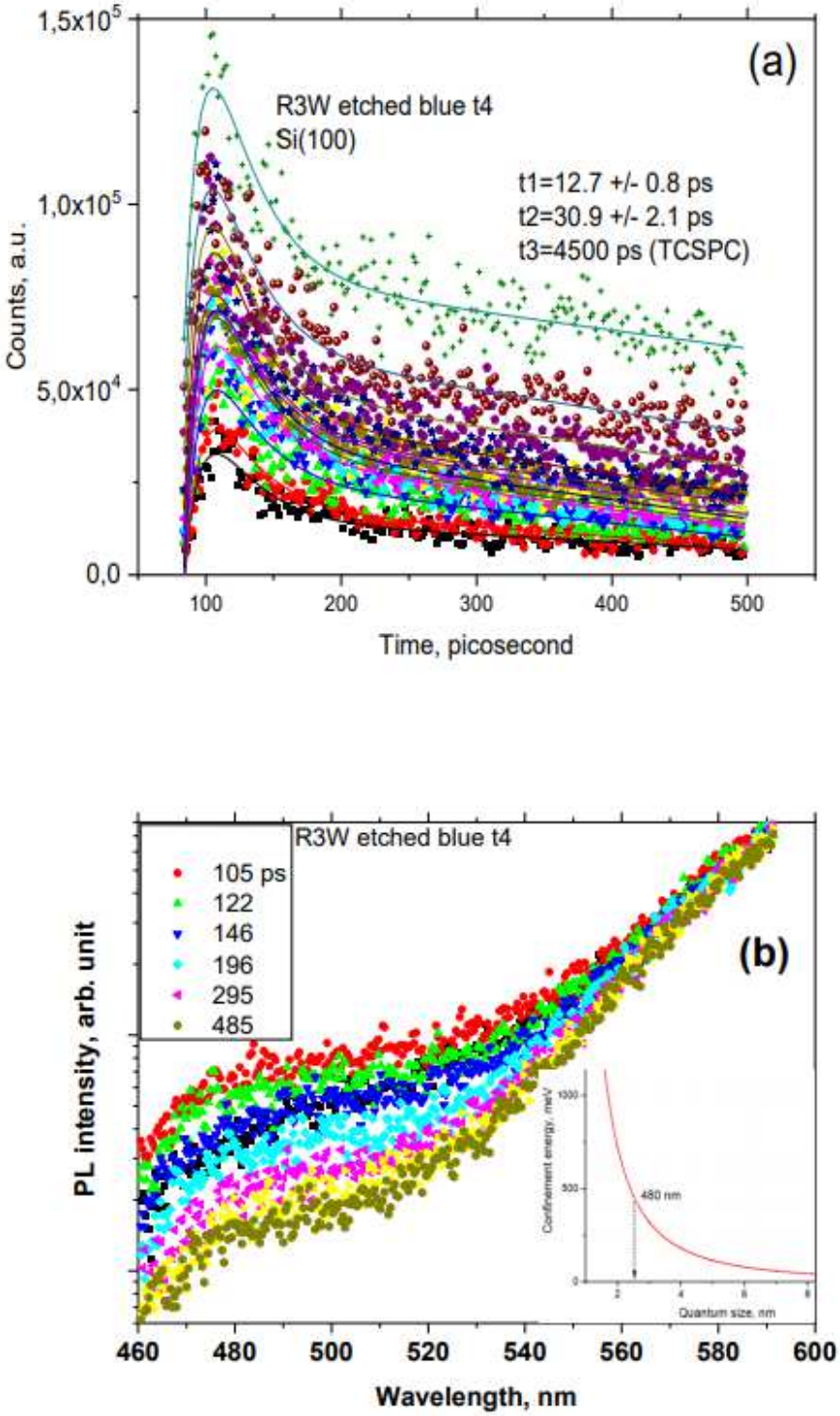

Figure 4

Room temperature excitation dynamics at 300 K for quantum pillars treated by HF:HNO3 vapors. a, Time-resolved PL stretching spectra integrated from 450 nm to 600 nm of b-Si. The solid red lines indicate a global fitting of the dynamics to a triple exponential decay functions. b, Spectral distribution of PL spectra between 470 nm and 600 nm as taken at different times.

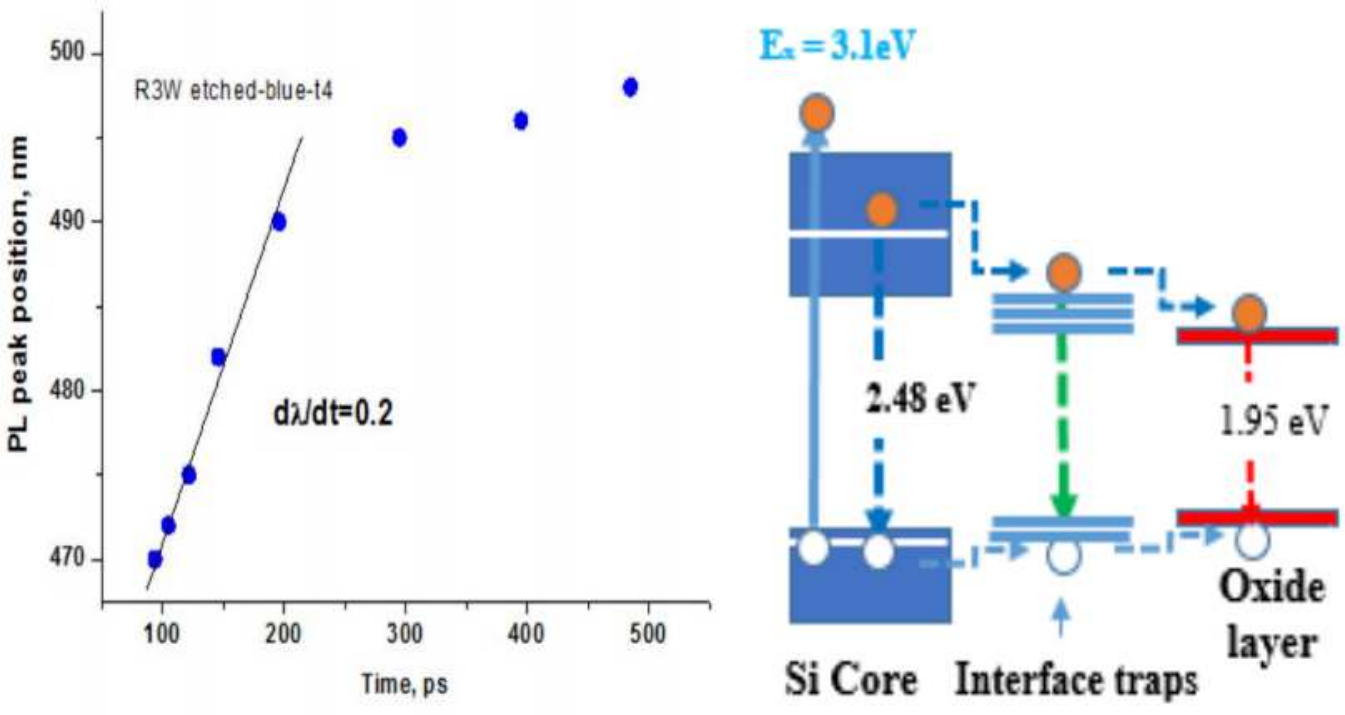

Figure 5

First derivative of the peak position versus decay-time. a, PL peak position as a function of decay time exhibits two slopes for the change. The change rate □□ □□ ⁄ = 0.2 over fast states is much higher than that for the slower states, that is □□ □□ ⁄ = 0.019, which is the typical characteristic of the slower states. b, Energy band diagram indicating the involvement of three states taking part in the recombination kinetics. The left hand side is the silicon core where the blue-green emission at around 2.5 eV occur due to the confinement effect; the middle part indicates traps involved recombination due to localized states between the core and the surface oxide; the right hand side is the red recombination originating from the oxide around the pillars.